ORGANIC SYNTHESIS

Synthesis of many different types of organic small molecules using one automated process

Junqi Li,* Steven G. Ballmer,* Eric P. Gillis, Seiko Fujii, Michael J. Schmidt, Andrea M. E. Palazzolo, Jonathan W. Lehmann, Greg F. Morehouse, Martin D. Burke†

Small-molecule synthesis usually relies on procedures that are highly customized for each target. A broadly applicable automated process could greatly increase the accessibility of this class of compounds to enable investigations of their practical potential. Here we report the synthesis of 14 distinct classes of small molecules using the same fully automated process. This was achieved by strategically expanding the scope of a building block–based synthesis platform to include even C_{sp3}-rich polycyclic natural product frameworks and discovering a catch-and-release chromatographic purification protocol applicable to all of the corresponding intermediates. With thousands of compatible building blocks already commercially available, many small molecules are now accessible with this platform. More broadly, these findings illuminate an actionable roadmap to a more general and automated approach for small-molecule synthesis.

Small molecules perform many important functions in nature, medicine, and technology. However, efforts to discover and optimize new small-molecule function are often impeded by limitations in synthetic access to this class of compounds. For peptides (*1*) and oligonucleotides (*2*), the development of automated synthesis platforms removed this bottleneck. The resulting expanded access to these molecules permitted widespread exploration and applications of their functional potential. Substantial progress has also been made toward automating the synthesis of oligosaccharides (*3*). In each of these cases, automation was enabled by the development of a general building block–based synthesis strategy and a common purification process for the corresponding intermediates. Such standardization reduced the number of processes employed and thus decreased the number of challenges involved in automating the synthesis platform. In contrast, despite tremendous progress in the field, small-molecule syntheses typically employ strategies and purification methods that are highly customized for each target, thus requiring automation solutions to be developed on an ad hoc basis (*4*–*7*). To enable the more generalized automation of small-molecule synthesis, we asked whether many different types of small molecules could be prepared using a common building block–based strategy and a common purification process.

Small molecules can be very diverse in structure, as illustrated by representative compounds **1** to **14** in Fig. 1A. Synthesis of this entire set of targets using a common approach thus represents a major challenge. However, like peptides, oligonucleotides, and oligosaccharides, most natural products (such as **1** to **4**) are biosynthesized via the iterative assembly of a small set of building blocks, such as malonyl coenzyme A, isopentenyl pyrophosphate, and pyruvic acid (*8*). Many materials and pharmaceuticals (such as **5** to **9**) comprise collections of aryl and/or heteroaryl components (*9*). Even topologically complex natural products containing macrocyclic or polycyclic frameworks (such as **10** to **14**) are usually biosynthesized via an iterative building block–based assembly of linear precursors, which are then (poly)cyclized to yield more complex molecular architectures (*10*–*12*). This analysis suggests that many small molecules might be accessible via a common, biosynthesis-inspired strategy involving the iterative assembly of building blocks. Supporting this notion, we recently demonstrated that more than 75% of all polyene natural product motifs can be prepared using just 12 building blocks and one coupling reaction (*13*).

That study employed a synthesis platform analogous to iterative peptide coupling that sequentially assembles bifunctional *N*-methyliminodiacetic acid (MIDA) boronates (Fig. 1B) (*14*). Iterative cycles of coupling and deprotection are enabled by the MIDA ligand, which attenuates the reactivity of boronic acids and thus prevents undesired oligomerization. This approach is both efficient and flexible because all of the required functional groups, oxidation states, and stereochemical elements are preinstalled into the building blocks. These features are then faithfully translated into the products using the same mild and stereospecific coupling chemistry (*15*). Hundreds of MIDA boronates and thousands of additional halide and boronic acid building blocks are now commercially available, and natural products from most major biosynthetic pathways, including **1** to **4**, have been manually synthesized in prior studies using this strategy (*16*–*19*).

With this promising starting point, we set out to expand the scope of this platform to include all of the structures shown in Fig. 1A. C_{sp3}-rich cyclic and polycyclic natural product frameworks such as **10** to **14** represent especially challenging targets and thus required a strategic advance. Because many of these molecules are biosynthesized via cyclization of modular linear precursors derived from iterative building block assembly (*10*–*12*), we hypothesized that an analogous linear-to-cyclized strategy might enable this platform to access many such structures. In this approach, the same building block assembly process is used to generate a linear precursor, which is then (poly)cyclized into the topologically complex product. The stereochemical information in the building blocks is first translated into linear precursors via stereospecific couplings and then into the targeted products via stereospecific and/or stereoselective (poly)cyclization reactions. To enable such cyclizations, such linear precursors must be suitably flexible and, therefore, rich in sp^3 hybridized carbons. Building block–based assembly of these precursors thus requires many C_{sp3} couplings, which can be challenging.

To test this linear-to-cyclized strategy, we targeted the manual synthesis of the highly complex pentacyclic secodaphnane alkaloid core **14**. This core can, in theory, be derived from a much simpler linear precursor **15** via a bioinspired cyclization cascade involving amine condensation and intramolecular Diels-Alder and Prins cyclizations (*20*). In turn, **15** was targeted via the iterative assembly of building blocks **16** to **18** in which all of the required double bond stereochemistry is preinstalled. C_{sp3} coupling of **16** and **17** generates MIDA boronate intermediate **19**. Deprotection of **19** yields a free boronic acid, which is engaged in another C_{sp3} coupling with **18** to complete the iterative assembly of linear precursor **15**. The aforementioned diastereoselective cyclization cascade is then used to transform **15** into the pentacyclic alkaloid (±)-**14**.

Having established a strategy to access even topologically complex small molecules using the same building block–based approach, we next questioned whether a common purification protocol could also be developed and thereby enable this platform to be automated. Small-molecule synthesis typically involves purifications customized for each intermediate, such as chromatography with eluents optimized for each compound. Such customization is incompatible with generalized automated purification. Solid-phase synthesis can address this problem for peptides (*1*), oligonucleotides (*2*), oligosaccharides (*3*), and some organic polymers (*21*). In some cases, syntheses of natural products and pharmaceuticals have also been aided by solid-phase methods (*22*). This approach is well established, is compatible with a wide range of chemistries, and has been employed in industry (*23*). However, small molecules do not possess a common functional group handle for attachment to solid support, which precludes generalized application of this approach. Thus, we needed a different solution.

Howard Hughes Medical Institute (HHMI), Department of Chemistry, University of Illinois at Urbana-Champaign, Urbana, IL 61801, USA.
*†These authors contributed equally to this work. †Corresponding author. E-mail: mdburke@illinois.edu

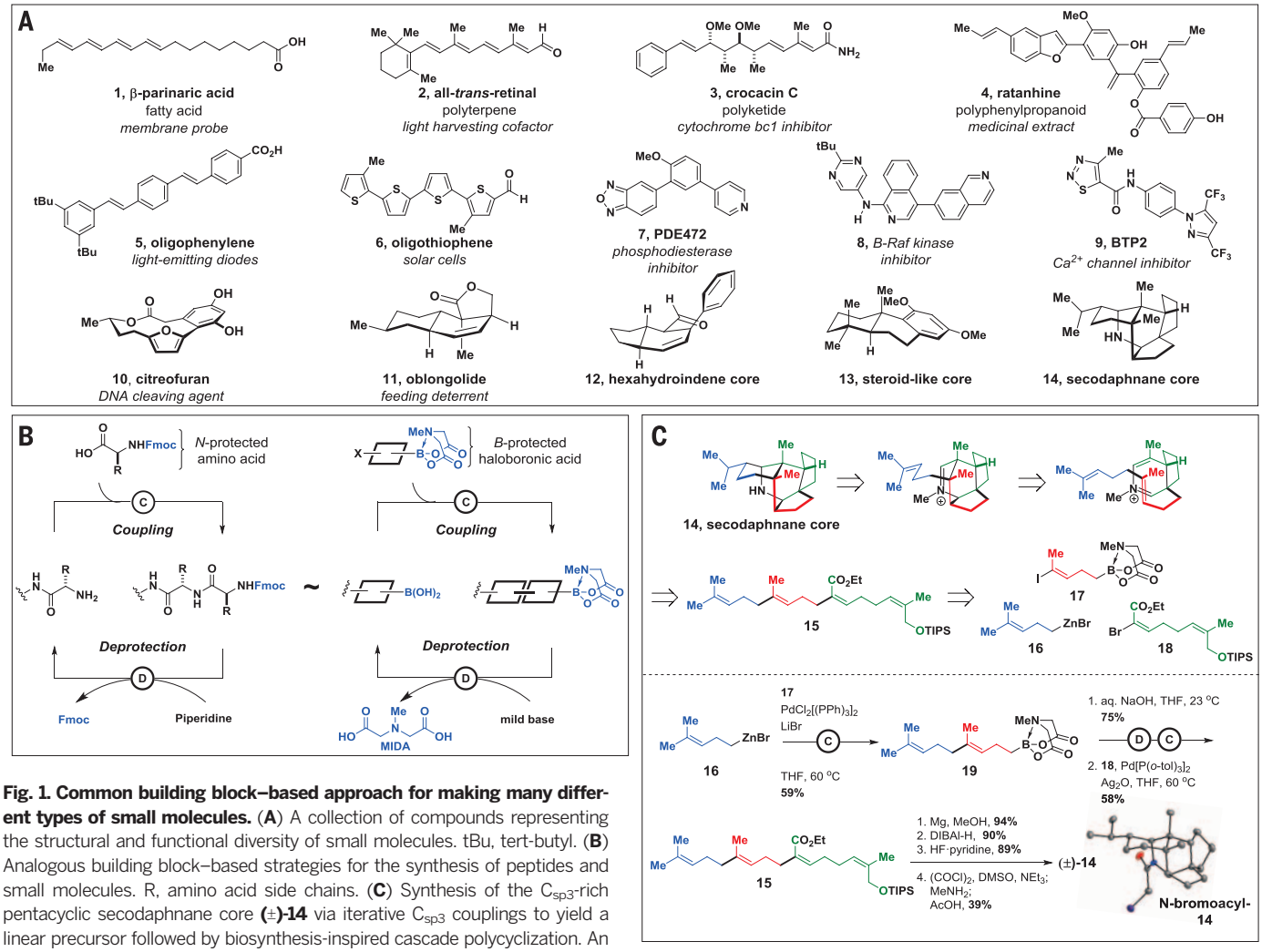

Fig. 1. Common building block–based approach for making many different types of small molecules. (**A**) A collection of compounds representing the structural and functional diversity of small molecules. tBu, tert-butyl. (**B**) Analogous building block–based strategies for the synthesis of peptides and small molecules. R, amino acid side chains. (**C**) Synthesis of the C_{sp3}-rich pentacyclic secodaphnane core **(±)-14** via iterative C_{sp3} couplings to yield a linear precursor followed by biosynthesis-inspired cascade polycyclization. An x-ray crystallographic study of the *N*-bromoacyl derivative of **14** unambiguously confirmed the structure of **14**. TIPS, triisopropylsilyl; Ph, phenyl; DMSO, dimethyl sulfoxide.

We recognized that each iteration of building block assembly in our platform generates a MIDA boronate as the key intermediate (Fig. 1, B and C). This led us to question whether the MIDA boronate motif could serve as a surrogate common handle for purification. In this vein, we discovered that MIDA boronates uniformly possess highly unusual binary affinity for silica gel with certain pairs of eluents (Fig. 2A). Specifically, all MIDA boronates **20** to **39**, with appended fragments representing a wide range of sizes, polarities, and functional group content, show minimal mobility on thin-layer silica gel chromatography when eluting with MeOH:Et_2O (Me, methyl; Et, ethyl) (Fig. 2A, left). However, all of the same MIDA boronates are rapidly eluted with tetrahydrofuran (THF) (Fig. 2A, right). This phenomenon enabled us to develop a new type of catch-and-release purification protocol applicable to any intermediate that contains a MIDA boronate. A crude reaction mixture is passed over silica gel, and the MIDA boronate is temporarily caught while excess reagents and by-products are removed via washing with MeOH:Et_2O. The MIDA boronate is then cleanly released by switching the eluent to THF. The MIDA boronate motif can thus serve as both a latent reactive functional group for iterative coupling and a traceless common functional group handle for generalized purification.

With both a common building block–based synthesis platform and a common purification method, we designed and built a synthesizer that iteratively assembles MIDA boronate building blocks in a fully automated fashion (Fig. 2B) (*24*). This device comprises three modules that sequentially execute the deprotection, coupling, and purification steps required for each cycle. All solutions are automatically transferred via computer-controlled syringe pumps running custom-designed software. Thus, each automated synthesis simply requires placing prepacked cartridges onto the synthesizer and pressing "start."

The fully automated synthesis commences at the deprotection module, where THF and water are syringed into a cartridge containing the MIDA boronate and NaOH. After deprotection, the reaction is quenched and the resulting THF solution of the freshly prepared boronic acid is separated from the water-soluble MIDA ligand. The coupling module then heats and stirs a solution of the next building block and the coupling reagents. The synthesizer then adds the freshly prepared solution of boronic acid to the coupling reaction. At the end of the reaction, the synthesizer filters and transfers the crude reaction mixture to the purification module, which executes the catch-and-release purification protocol with MeOH:Et_2O followed by THF. The THF solution of the purified product is then transferred directly into the deprotection module to start the next iteration of the synthesis.

To first test the capacity of this synthesizer to execute one cycle of deprotection, coupling, and purification, we subjected a series of commercially available aryl, heteroaryl, and vinyl MIDA boronates to automated deprotection and coupling with a model bifunctional building block, 4-bromophenyl MIDA boronate (*24*) (table S2). Using a standard set of hydrolysis conditions (NaOH, THF:H_2O, 23°C, 20 min) and coupling conditions ($PdXPhos$, K_3PO_4) (*25*), we obtained the desired cross-coupling products in good yields and purities in all cases (table S2, entries 1 to 3). The synthesizer was also capable of executing a

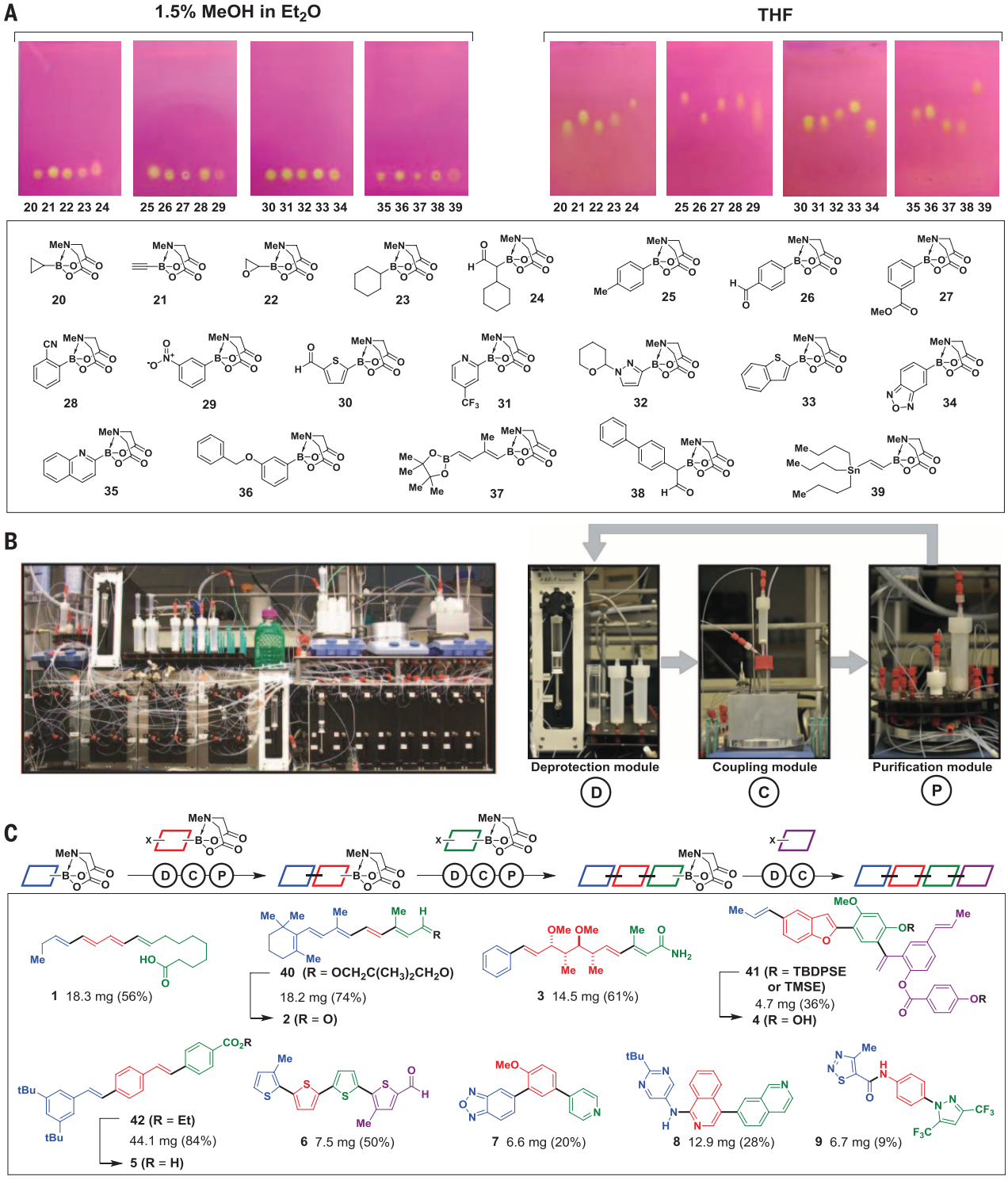

Fig. 2. General purification process to enable automation. (**A**) MIDA boronates uniformly show binary elution properties on silica gel thin-layer chromatography. (**B**) Photograph of the small-molecule synthesizer, which comprises three modules that execute the deprotection, coupling, and purification steps. (**C**) Automated synthesis of natural products, materials, pharmaceuticals, and biological probes via iterative coupling of building blocks indicated by different colors (*24*). TBDPSE, tert-butyldiphenylsilylethyl; TMSE, trimethylsilylethyl.

C_{sp3} coupling using Pd[P(*o*-tol$_3$)]$_2$ (tol, tolyl) and Ag_2O/K_2CO_3 (table S2, entry 4).

Accessing many pharmaceuticals and materials represented by structures **5** to **9** requires the flexibility to link building blocks via carbon-heteroatom and/or carbon-carbon bonds. The stability of MIDA boronates toward many reaction conditions (*26*, *27*) and the synthetic versatility of boronic acids (*28*) allowed us to add carbon-heteroatom bond formations to the same platform. The synthesizer successfully executed a series of automated carbon-heteroatom bond formations, including a Buchwald-Hartwig amination, O-alkylation, and amide bond formations (table S3). Despite the different reagents

and by-products, the same catch-and-release process purified all of the corresponding MIDA boronate products.

Having confirmed the capacity to reliably execute single cycles of deprotection, coupling, and purification, we next targeted the automated synthesis of a wide range of linear small molecules (**1** to **9**) via multiple carbon-carbon and/or carbon-heteroatom bond formations (Fig. 2C). These include natural products from major biosynthetic pathways (**1** to **4**), materials components (**5**, **6**), and pharmaceuticals and biological probes (**7** to **9**). Most of the corresponding building blocks are commercially available. Similar to automated peptide, oligonucleotide, and oligosaccharide syntheses, all of the synthesizer-generated final products were purified using standard chromatographic techniques, and any protecting groups other than MIDA were easily removed in a separate step (*24*). In each case, a single automated run successfully delivered the targeted small molecule in multi-milligram quantities, fulfilling the requirements of most functional discovery assays.

The development of small molecules with optimized functions often requires efficient access to many structural derivatives of a parent compound. To test if this platform could enable such access, we targeted the automated preparation of many derivatives of the complex neolignan natural product ratanhine **4**. In this experiment, we did not optimize any of the deprotection, coupling, or purification conditions used to construct **41** (Fig. 2C). We input four sets of building blocks representing common substructural elements found throughout the neolignan family and/or other pharmaceutically relevant motifs (Fig. 3). These building blocks included variations in oxidation states, methylation patterns, fluorine content, aromatic ring identity, and size. They also represent preprogrammed oligomer lengths of 3 to 4 units, based on whether the third building block was a bifunctional halo-MIDA boronate or a capping halide. In the event, the synthesizer successfully generated 20 out of 20 of the targeted derivatives, collectively representing all possible combinations of this four-component matrix of building blocks (Fig. 3).

Finally, we tested whether a wide range of macro- and polycyclic natural products and natural product–like cores (**10** to **14** in Fig. 1A) could be generated using the same automated building

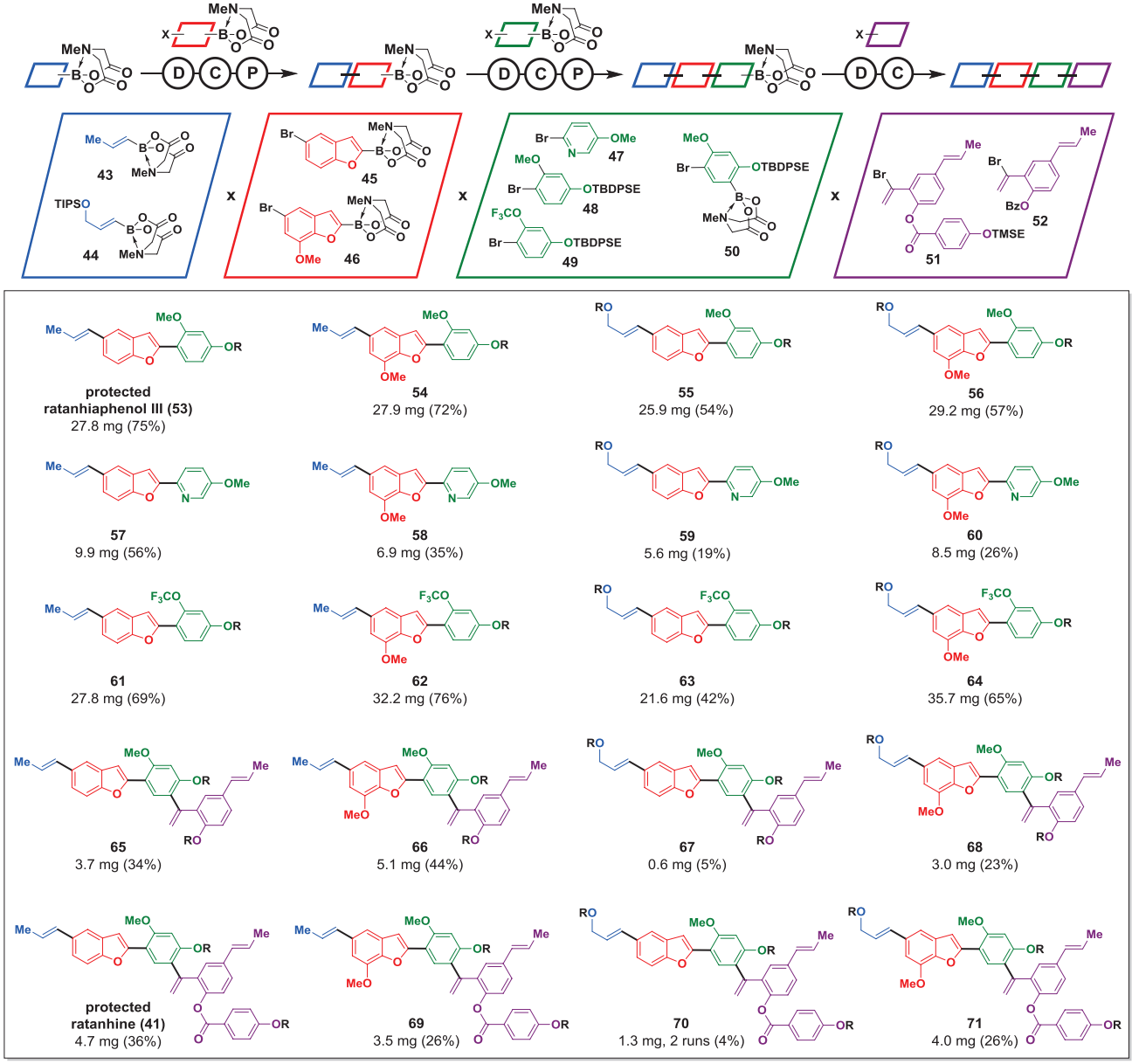

Fig. 3. Automated synthesis of ratanhine derivatives. Conditions: Deprotection – NaOH, THF:H_2O. Coupling – cycle 1: $Pd(OAc)_2$, SPhos, K_2CO_3, THF, 55°C, 16 hours; cycle 2: $Pd(OAc)_2$, XPhos, K_3PO_4, THF, 55°C, 14 hours; cycle 3: $Pd(OAc)_2$, SPhos, K_3PO_4, THF, 55°C, 24 hours. Purification – SiO_2, MeOH:Et_2O; THF. All protecting groups other than MIDA [R: TIPS, TBDPSE, TMSE, or Bz (benzoyl)] were successfully removed in a separate step (*24*). OAc, acetate.

block assembly process and the linear-to-cyclized strategy. The macrocyclic natural product citreofuran possesses both C_{sp3} and atropisomerism stereochemical elements (Fig. 4, entry 1). This complex target can be derived from linear precursor **76** (*29*), which can, in theory, be assembled from building blocks **72** to **74**. All of the required stereochemical information for citreofuran is preencoded in the chiral nonracemic MIDA boronate building block **72**. On the synthesizer, fully automated deprotection of **72**, C_{sp3} coupling with **73**, and purification yielded intermediate **75**. A second round of deprotection and coupling of the resulting 2-furanyl boronic acid with **74** produced linear precursor **76**. This linear precursor was then deprotected and atropdiastereoselectively macrocyclized to generate citreofuran.

Oblongolide is a norsesquiterpene γ-lactone natural product containing a 6,6,5-tricyclic core with five C_{sp3} stereogenic centers, one of which is quaternary (Fig. 4, entry 2). The three building blocks **44**, **77**, and **78** were automatically assembled via iterative C_{sp2} and C_{sp3} couplings to produce linear precursor **80**. After deprotection, the linear precursor was subjected to a cascade intramolecular substrate-controlled diastereoselective Diels-Alder reaction and lactonization process (*30*), which defined the four contiguous stereogenic centers in oblongolide.

In cases where no C_{sp3} stereogenic centers are present in the linear precursors, the enantioselectivity of cyclizations can be controlled using a rapidly expanding toolbox of chiral catalysts (*31*). This approach allows the stereoselective construction of the natural product–like hexahydroindene and steroid-like core structures **12** and **13** using the same linear-to-cyclized strategy (Fig. 4, entries 3 and 4). Specifically, building blocks **81** to **83**, all possessing olefins with predefined geometries required for cyclization, were assembled on the synthesizer to produce linear precursor **85**. This precursor was then subjected to deprotection and a chiral imidazolidinone-promoted organocatalytic enantio- and diastereoselective Diels-Alder reaction to generate **12** (Fig. 4, entry 3) (*32*). Similarly, iterative C_{sp3} coupling of building blocks **16, 17**, and **86** generated linear precursor **87**, which then underwent catalyst-promoted enantio- and diastereoselective cation-π cyclization (*33*) followed by reduction to generate **13** (Fig. 4, entry 4). Finally, by simply replacing building block **86** with **18** and using the same automated platform, even the highly complex pentacyclic secodaphnane core (±)-**14** was readily prepared (Fig. 4, entry 5).

Thus, many different types of small molecules (**1** to **14** in Fig. 1A) can be synthesized using one automated building block assembly platform. This advance was enabled by standardizing the synthesis and purification processes used to assemble these structures. Importantly, a majority of the building blocks employed herein are already commercially available.

Further expanding the scope of this automated synthesis platform represents an actionable roadmap toward a general and broadly accessible solution to the small-molecule synthesis problem. This roadmap includes creating building blocks representing the highly redundant

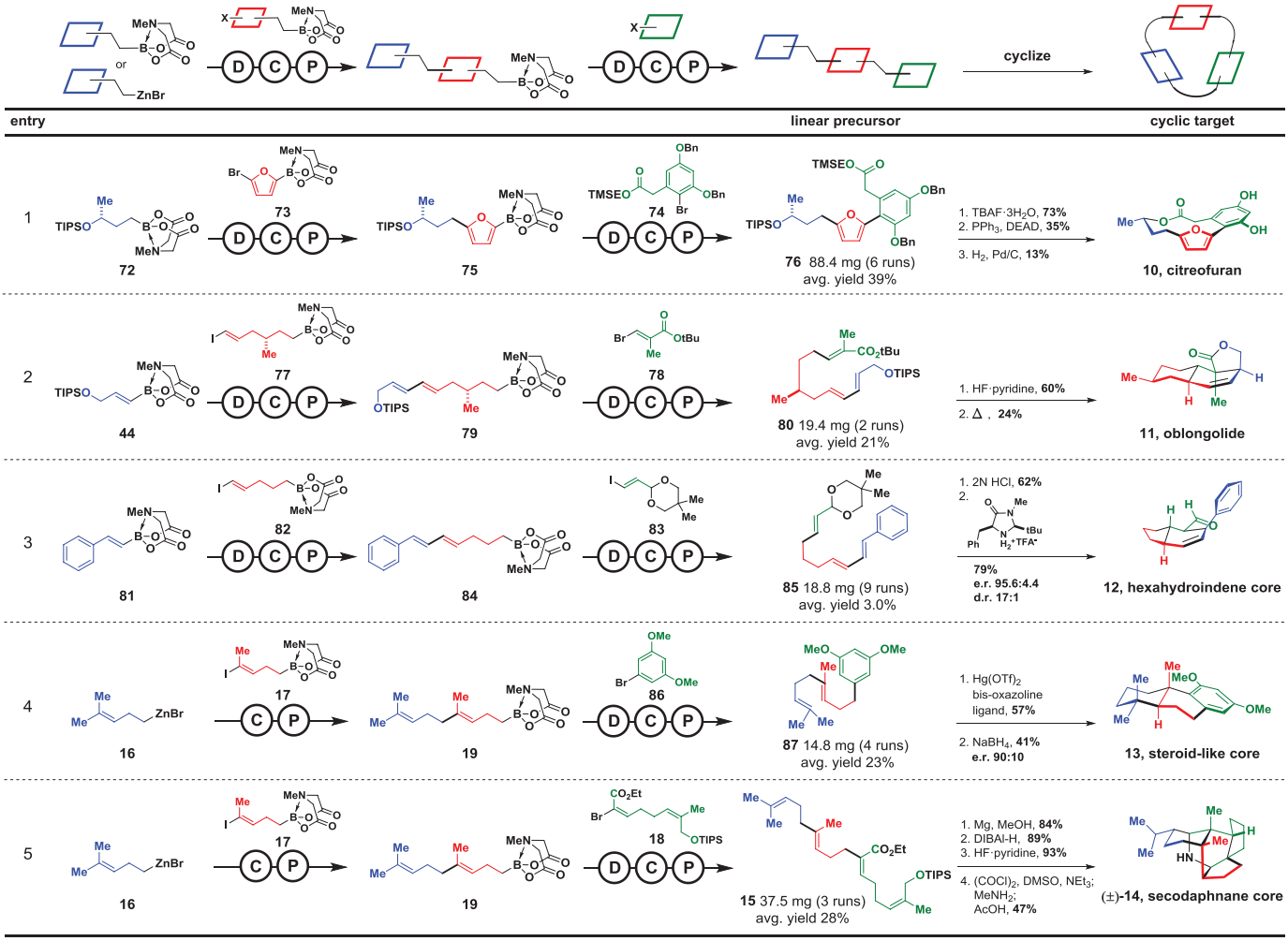

Fig. 4. Synthesis of C_{sp3}-rich macro- and polycyclic natural products and natural product–like cores. Modular linear precursors assembled via automated C_{sp2} and C_{sp3} couplings are diastereo- and/or enantioselectively cyclized. TBAF, tetra-*n*-butylammonium fluoride; DEAD, diethyl azodicarboxylate; OTf, trifluoromethanesulfonate; DIBAl-H, diisobutylaluminum hydride. e.r., enantiomeric ratio; d.r., diastereomeric ratio.

substructural elements found in many small molecules (*13*), developing better methods for iteratively coupling those building blocks together, and advancing the capacity for biosynthesis-inspired cyclizations of linear precursors to yield complex natural product frameworks. Achieving these objectives stands to better enable the scientific community to bring the substantial power of small-molecule synthesis to bear upon many important unsolved problems in society.

REFERENCES AND NOTES

1. R. B. Merrifield, *Science* **150**, 178–185 (1965).
2. M. H. Caruthers, *Science* **230**, 281–285 (1985).
3. O. J. Plante, E. R. Palmacci, P. H. Seeberger, *Science* **291**, 1523–1527 (2001).
4. S. V. Ley, D. E. Fitzpatrick, R. J. Ingham, R. M. Myers, *Angew. Chem. Int. Ed.* **54**, 10.1002/anie.201410744 (2015).
5. S. Fuse, K. Machida, T. Takahashi, in *New Strategies in Chemical Synthesis and Catalysis*, B. Pignataro, Ed. (Wiley, Weinheim, Germany, 2012), chap. 2.
6. A. G. Godfrey, T. Masquelin, H. Hemmerle, *Drug Discov. Today* **18**, 795–802 (2013).
7. S. Newton *et al*., *Angew. Chem. Int. Ed.* **53**, 4915–4920 (2014).
8. P. M. Dewick, *Medicinal Natural Products: A Biosynthetic Approach* (Wiley, West Sussex, UK, 2009).
9. E. Vitaku, D. T. Smith, J. T. Njardarson, *J. Med. Chem.* **57**, 10257–10274 (2014).
10. R. A. Yoder, J. N. Johnston, *Chem. Rev.* **105**, 4730–4756 (2005).
11. E. M. Stocking, R. M. Williams, *Angew. Chem. Int. Ed.* **42**, 3078–3115 (2003).
12. F. Kopp, M. A. Marahiel, *Nat. Prod. Rep.* **24**, 735–749 (2007).
13. E. M. Woerly, J. Roy, M. D. Burke, *Nat. Chem.* **6**, 484–491 (2014).
14. E. P. Gillis, M. D. Burke, *J. Am. Chem. Soc.* **129**, 6716–6717 (2007).
15. N. Miyaura, A. Suzuki, *Chem. Rev.* **95**, 2457–2483 (1995).
16. E. P. Gillis, M. D. Burke, *Aldrichim Acta* **42**, 17–27 (2009).
17. E. M. Woerly, A. H. Cherney, E. K. Davis, M. D. Burke, *J. Am. Chem. Soc.* **132**, 6941–6943 (2010).
18. K. C. Gray *et al*., *Proc. Natl. Acad. Sci. U.S.A.* **109**, 2234–2239 (2012).
19. K. Fujita, R. Matsui, T. Suzuki, S. Kobayashi, *Angew. Chem. Int. Ed.* **51**, 7271–7274 (2012).
20. C. H. Heathcock, S. Piettre, R. B. Ruggeri, J. A. Ragan, J. C. Kath, *J. Org. Chem.* **57**, 2554–2566 (1992).
21. E. L. Elliott, C. R. Ray, S. Kraft, J. R. Atkins, J. S. Moore, *J. Org. Chem.* **71**, 5282–5290 (2006).
22. M. Mentel, R. Breinbauer, *Top. Curr. Chem.* **278**, 209–241 (2007).
23. S. Maechling, J. Good, S. D. Lindell, *J. Comb. Chem.* **12**, 818–821 (2010).
24. Materials and methods are available as supplementary materials on *Science* Online.
25. T. Kinzel, Y. Zhang, S. L. Buchwald, *J. Am. Chem. Soc.* **132**, 14073–14075 (2010).
26. E. P. Gillis, M. D. Burke, *J. Am. Chem. Soc.* **130**, 14084–14085 (2008).
27. J. E. Grob *et al*., *Org. Lett.* **14**, 5578–5581 (2012).
28. D. G. Hall, Ed., *Boronic Acids: Preparation and Applications in Organic Synthesis, Medicine and Materials* (Wiley, Weinheim, Germany, 2011).
29. F. Bracher, B. Schulte, *Nat. Prod. Res.* **17**, 293–299 (2003).
30. T. K. M. Shing, J. Yang, *J. Org. Chem.* **60**, 5785–5789 (1995).
31. E. J. Corey, L. Kürti, in *Enantioselective Chemical Synthesis: Methods, Logic, and Practice* (Direct Book Publishing, Dallas, TX, 2010), pp. 121–151.
32. R. M. Wilson, W. S. Jen, D. W. C. Macmillan, *J. Am. Chem. Soc.* **127**, 11616–11617 (2005).
33. S. A. Snyder, D. S. Treitler, A. Schall, *Tetrahedron* **66**, 4796–4804 (2010).

ACKNOWLEDGMENTS

We acknowledge the NIH (grants GM080436 and GM090153), the NSF (grant 0747778), HHMI, and Bristol-Myers Squibb for funding. M.D.B. is an HHMI Early Career Scientist, J.L. was an HHMI International Student Research Fellow, and J.L. and E.P.G. were Bristol-Myers Squibb Graduate Fellows. We thank D. Gray for performing the x-ray analysis on **N-bromoacyl-14**. The University of Illinois has filed patent applications on MIDA boronate chemistry and the automated synthesis platform reported herein. These inventions have been licensed to REVOLUTION Medicines, a company for which M.D.B. is a founder. Metrical parameters for the structure of **N-bromoacyl-14** are available free of charge from the Cambridge Cyrstallographic Data Centre under reference CCDC-1045844.

SUPPLEMENTARY MATERIALS

www.sciencemag.org/content/347/6227/1221/suppl/DC1
Materials and Methods
Supplementary Text
Figs. S1 to S14
Tables S1 to S3
References (*34*–*52*)

22 December 2014; accepted 12 February 2015
10.1126/science.aaa5414

LUNAR GEOLOGY

A young multilayered terrane of the northern Mare Imbrium revealed by Chang'E-3 mission

Long Xiao,[1,2]* Peimin Zhu,[1]* Guangyou Fang,[3]* Zhiyong Xiao,[1,4] Yongliao Zou,[5] Jiannan Zhao,[1] Na Zhao,[1] Yuefeng Yuan,[1] Le Qiao,[1] Xiaoping Zhang,[2] Hao Zhang,[1] Jiang Wang,[1] Jun Huang,[1] Qian Huang,[1] Qi He,[1] Bin Zhou,[3] Yicai Ji,[3] Qunying Zhang,[3] Shaoxiang Shen,[3] Yuxi Li,[3] Yunze Gao[3]

China's Chang'E-3 (CE-3) spacecraft touched down on the northern Mare Imbrium of the lunar nearside (340.49°E, 44.12°N), a region not directly sampled before. We report preliminary results with data from the CE-3 lander descent camera and from the Yutu rover's camera and penetrating radar. After the landing at a young 450-meter crater rim, the Yutu rover drove 114 meters on the ejecta blanket and photographed the rough surface and the excavated boulders. The boulder contains a substantial amount of crystals, which are most likely plagioclase and/or other mafic silicate mineral aggregates similar to terrestrial dolerite. The Lunar Penetrating Radar detection and integrated geological interpretation have identified more than nine subsurface layers, suggesting that this region has experienced complex geological processes since the Imbrian and is compositionally distinct from the Apollo and Luna landing sites.

Chang'E-3 (CE-3) landed at 340.49°E, 44.12°N on the Moon on 14 December 2013, and it released the Yutu (Jade Rabbit) rover the next morning (*1*). This was the first soft landing on the Moon since the Soviet Union's Luna 24 mission in 1976 and is a new landing site in the north part of the Mare Imbrium (fig. S1). Yutu is China's first lunar geologic mission and traveled in total ~114 m on the lunar surface. Following a zigzagging route, Yutu came to a halt about 20 m to the southwest of the landing site (Fig. 1). Yutu explored the lunar surface and subsurface near a young crater (fig. S2) using its four main instruments: Panoramic Camera, Lunar Penetrating Radar (LPR), Visible–Near Infrared Spectrometer (VNIS), and Active Particle-Induced X-ray Spectrometer (APXS). In this study, we report the preliminary results obtained from the cameras and LPR.

[1]China University of Geosciences, Wuhan 430074, China. [2]Macau University of Science and Technology, Macau, China. [3]Institute of Electronics, China Academy of Science, Beijing 100190, China. [4]The Centre for Earth Evolution and Dynamics, University of Oslo, Sem Sælandsvei 24, 0371 Oslo, Norway. [5]National Astronomical Observatories, China Academy of Science, Beijing 100012, China.
***Corresponding author. E-mail: longxiao@cug.edu.cn (L.X.); zhupm@cug.edu.cn (P.Z.); gyfang@mail.ie.ac.cn (G.F.)**

High-resolution images returned by both Yutu and the lander show that the landing site features thin regolith and numerous small craters that are centimeters to tens of meters in diameter (Fig. 1 and figs. S3 to S6). Although at the regional scale the mare surface at the landing site appears relatively flat, the landing site is located ~50 m from the eastern rim of the ~450-m crater (C_1) (*2*). The traversed area of the Yutu rover was wholly restricted within the continuous ejecta deposits (fig. S2). Crater size-frequency distribution measurements (*2*) for the continuous ejecta deposits of the C_1 crater yield a minimum model age of ~27 million years (My) and a maximum model age of ~80 My, which is late Copernican (*3*), consistent with the estimation made from the preservation state of the crater and from the meter-sized boulders observed on the crater rim (*2*).

Yutu drove very close to the rim of the C_1 crater, and its panoramic cameras photographed the shape and interior features of the crater. A full image of the crater was also acquired (fig. S4A) when Yutu stood behind the Loong rock (position number 13 in Fig. 1) (*1*). This circular-rimmed crater has distinct rocky walls and rims, except on the northern side. The ejected boulders are

Science
AAAS

Synthesis of many different types of organic small molecules using one automated process

Junqi Li *et al.*

Science **347**, 1221 (2015);
DOI: 10.1126/science.aaa5414